Thin Solid Films 519 (2010) 31–36

Contents lists available at ScienceDirect

Thin Solid Films

journal homepage: www.elsevier.com/locate/tsf

Room temperature deposition of Al-doped ZnO films on quartz substrates by radio-frequency magnetron sputtering and effects of thermal annealing

Weifeng Yang [a], Zhengyun Wu [a,*], Zhuguang Liu [a], Aisuo Pang [a], Yu-Li Tu [b], Zhe Chuan Feng [b,*]

[a] Department of Physics, Xiamen University, Xiamen 361005, PR China

[b] Department of Electrical Engineering, National Taiwan University, Taipei 106-17, Taiwan

ARTICLE INFO

Article history:
Received 23 May 2009
Received in revised form 1 July 2010
Accepted 9 July 2010
Available online 16 July 2010

Keywords:
Aluminum oxide
Hall effect
Optical properties
Quartz
Sputtering
X-ray diffraction
X-ray photoelectron spectroscopy (XPS)
Zinc oxide

ABSTRACT

High-quality Al-doped zinc oxide (AZO) thin films have been deposited on quartz substrates by radio-frequency magnetron sputtering at room temperature for thin film solar cell applications as transparent conductive oxide (TCO) electrode layers. Effects of post-deposition annealing treatment in pure nitrogen and nitrogen/hydrogen atmosphere have been investigated. Annealing treatments were carried out from 300 °C to 600 °C for compatibility with typical optoelectronic device fabrication processes. A series of characterization techniques, including X-ray diffraction, scanning electron microscopy, Hall, optical transmission, and X-ray photoelectron spectroscopy has been employed to study these AZO materials. It was found that there were significant changes in crystallinity of the films, resistivity increased from 4.60×10^{-4} to 4.66×10^{-3} Ω cm and carrier concentration decreased from 8.68×10^{20} to 2.77×10^{20} cm^{-3} when annealing in 400 °C pure nitrogen. Whereas there were no significant changes in electrical and optical properties of the AZO films when annealing in 300–500 °C nitrogen/hydrogen atmosphere, the electrical stability of the AZO films during the hydrogen treatment is attributed to both desorption of adsorbed oxygen from the grain boundaries and production of additional oxygen vacancies that act as donor centers in the films by removal of oxygen from the ZnO matrix. These results demonstrated that the AZO films are stably suited for TCO electrodes in display devices and solar cells.

© 2010 Elsevier B.V. All rights reserved.

1. Introduction

Heavily doped ZnO films have recently been recognized as a potential replacement transparent conductive oxide to the industry standard tin-doped indium oxide (ITO). They are transparent at visible wavelength ranges, have direct and wide band gap (E_g>3.30 eV at room temperature), and have a large exciton binding energy (~60 meV at room temperature). Such properties make ZnO well suited for the realization of many optoelectronic applications including transparent conductive oxides in display devices and solar cells [1–4]. Recent researches demonstrated that B, Al, Ga, In, and F doped ZnO films reveal both low resistivity and high transmittance in the visible region [5–8]. Among these, Al-doped ZnO (AZO) has similar electrical and optical properties to ITO, but comparing to which, AZO possesses advantages of a nontoxic material, with high temperature stability, and costs less to manufacture [9].

Different technologies such as electron beam evaporation [10], sol–gel [11], chemical spray [12], pulsed laser deposition [13], direct-current and radio-frequency (RF) magnetron sputtering [14], etc. have been reported to produce thin films of AZO with adequate performance for applications. However, these deposition techniques, while yielding high-quality films, require relatively high temperatures [14,15], which are incompatible with plastic substrates or sensitive photoresist as those used in light emitting diodes and solar cells, especially in lift-off fabrication technology. Moreover, there are some reports [16–20] on annealing of the AZO films deposited at high temperature substrate, but yet there are very few reports on annealing of the AZO films deposited at room temperature (RT). In this paper, high performance AZO thin films were grown by RF magnetron sputtering RT, and a systematic study of annealing effects on the structural, electrical, and optical properties of the AZO thin films in different temperatures and different atmospheres has been discussed in detail.

2. Experimental details

The AZO films were deposited on quartz substrates in a SP-2 RF magnetron sputtering system with a base pressure of 4×10^{-4} Pa and at RT. A sintered ceramic sputter target with a mixture of ZnO (99.99% purity) and Al_2O_3 (99.99% purity) was employed as source material. The content of Al_2O_3 added to the sputter target was 2% in weight. The sputtering power, Ar flow rate, and the distance between sputter target and substrate were optimized at 300 W, 30 sccm, and 7 cm, respectively. Details of the AZO deposition process have been reported elsewhere [21]. The as-deposited AZO films were subsequently conventionally heat-treated for 15 min in pure N_2 and N_2 with 4% hydrogen atmosphere by varying the annealing temperature from

* Corresponding authors. Tel.: +886 2 3366 3543; fax: +886 2 2367 7467.
E-mail addresses: zhywu@xmu.edu.cn (Z. Wu), fengzc@cc.ee.ntu.edu.tw (Z.C. Feng).

0040-6090/$ – see front matter © 2010 Elsevier B.V. All rights reserved.
doi:10.1016/j.tsf.2010.07.048

300 °C to 600 °C. This temperature was chosen since it is known as the maximum range in typical device processing.

A series of analytical technologies was employed to characterize and investigate the polycrystalline AZO materials. The structural properties of the AZO films were analyzed with a Panalytical X'pert PRO powder X-ray diffractometer which uses a Cu-Kα radiation ($\lambda = 0.15406$ nm). The surface morphology and section shape of the AZO films were examined by using a field emission scanning electron microscopy (SEM) LEO 1530. The optical transmission spectra of the AZO films were measured from a Cary 5000 spectrophotometer. The film thickness was determined through a Dektak3 surface profile measurement system. The resistivity, carrier concentration and carrier mobility of the AZO films were acquired by way of an Accent HL5500 Hall System with a four-point probe. The chemical state in the films was investigated by means of X-ray photoelectron spectroscopy (XPS) using a PHI Quantum 2000 Scanning ESCA Microprobe instrument.

3. Results and discussion

3.1. Structural features studied via X-ray diffraction

Fig. 1 shows X-ray diffraction (XRD) patterns for the AZO thin films, as-grown and annealed from 300 °C to 600 °C in N_2 and $N_2 + 4\%$ H_2 atmosphere, respectively. All of the AZO thin films gave strong (002) diffraction peaks. Other peaks (004) with much less intensity were observed, with no obvious metallic zinc, aluminum, or ZnAlO characteristic peaks found. These indicate that all the experimental AZO films grown on quartz substrates exhibit a strong c-axis orientation perpendicular to the substrate surface.

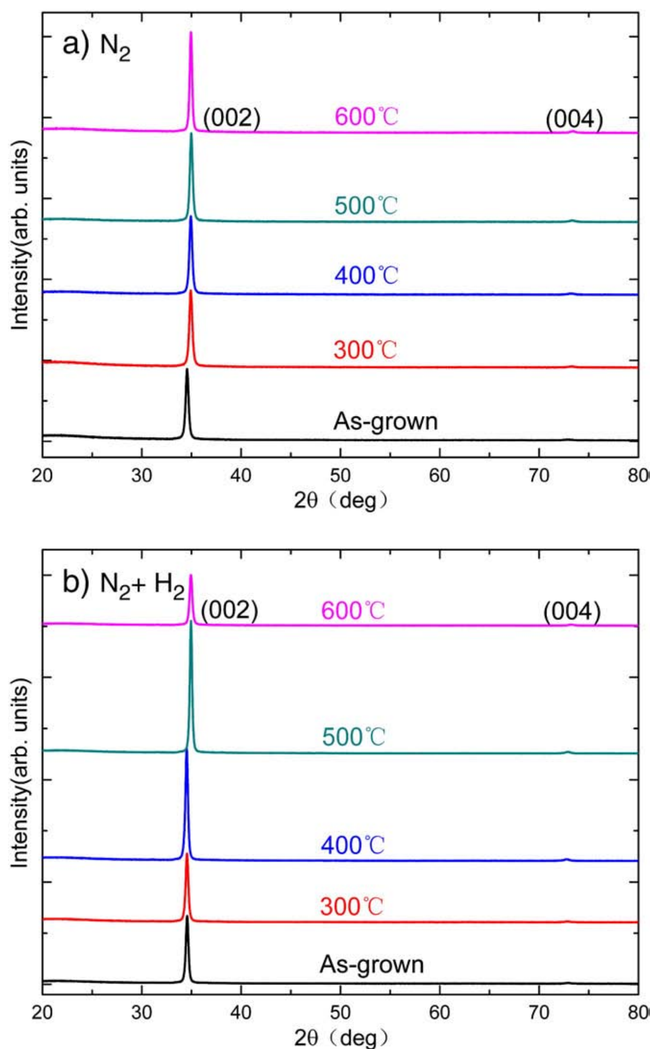

Fig. 1. XRD patterns of the as-grown and post-annealed AZO films at 300 °C–600 °C for 15 min in (a) N_2, and (b) $N_2 + 4\%$ H_2.

To compare the structure features of the AZO films, the full-width at half-maximum (FWHM) of the XRD (002) peak and the crystallite dimension are listed in Table 1. The FWHM values for AZO/quartz were found to decrease from 0.271 to 0.262° as annealed in N_2 from 300 °C to 600 °C and decreased to 0.265° for annealed in $N_2 + H_2$ from 300 °C to 500 °C, while increased to 0.283° at 600 °C.

The grain size of the films can be calculated according to Scherrer relation [20]:

$$D = (0.9\lambda) / \beta \cos\theta \quad (1)$$

where λ is the X-ray wavelength, 0.154 nm, and $\beta = B - b$ where B is the observed FWHM and b is the instrument function parameter determined from the broadening of the monocrystalline silicon diffraction peak. The obtained grain size (D) values for the experimental AZO films are listed in Table 1, being in range of 30.5–35.2 nm. For the samples annealed in N_2, D increased slightly from as-grown one to annealing till 400 °C, and reached a highest value of 35.2 nm for annealing at 600 °C. For annealing in $N_2 + H_2$, D also increased from as-grown one to annealing till 500 °C, reached a highest value of 34.8 nm for annealing at 500 °C, but decreased to a low value of 30.5 nm at 600 °C. The grain size values have showed similar trend with the annealing conditions as XRD FWHM does.

The improvement in crystallinity by annealing may be explained by the increase in grain size and the decrease of point defects such as oxygen vacancy and zinc interstitial as the annealing temperature increases. While the weakening in crystallinity by annealing at 600 °C in $N_2 + H_2$ could be due to the decrease of grain size and destruction of film surface perfection which were resulted from oxygen species on surface combined by hydrogen contamination atoms.

3.2. Surface morphology and status

The surface morphologies of the as-grown and post-annealed AZO thin films were examined by SEM and are shown in Fig. 2. The films are composed of closely packed nanocrystallites. The grain size of the as-grown AZO film is directly seen to increase with increasing annealing temperature in N_2 as revealed from XRD data analysis in the last section. Different morphologies were observed for the AZO films grown on quartz with increasing annealing temperature. Fig. 2b) shows the cross-sectional SEM micrograph of the as-grown sample. The film grows in a columnar structure vertical to the substrate, being consistent with the XRD measurement results (c-axis orientation). However, the upper section of the fracture edge does not show this clear structure, which was possibly caused by the destruction during the cutting process. Porous surface was found on the AZO thin films when annealing at 600 °C in $N_2 + 4\%$ H_2, as shown in Fig. 2f), which

Table 1
The structural properties and atomic percent for the AZO films as-deposited and annealed in different atmospheres.

Sample	002 peak (°)	FWHM (°)	Grain size (nm)	O (at.%)	Zn (at.%)	Al (at.%)
As-deposited	34.55	0.271	33.0	47	50	3
N_2, 400 °C	34.94	0.271	33.1	42	55	3
$N_2 + H_2$, 400 °C	34.57	0.270	33.3	48	49	3
N_2, 600 °C	34.96	0.262	35.2	41	56	3
$N_2 + H_2$, 600 °C	34.94	0.283	30.5	45	53	3

Fig. 2. SEM images of the AZO thin films as-grown and annealed at different temperatures in different atmospheres.

implies that the N_2+H_2 atmosphere has apparently etched the film significantly and possibly made the films thinner.

The XPS spectra were recorded with PHI 2000 spectrometer using Al (1486.6 eV) radiation. The spectra were referenced to the surface impurity C 1s line (284.8 eV) binding energy. The quantitative analysis was done by using XPS spectra obtained at a depth of about 50 nm from the film surface. Fig. 3 exhibits XPS wide scans for the AZO films on quartz of as-grown, annealed at 400, 500 and 600 °C in the N_2, respectively. From XPS narrow scans (not shown here) and analyses on the peaks of Zn $2p_{3/2}$ at ~1022 eV, O 1s at ~531 eV and Al 2p at ~74 eV, respectively, atomic ratios of element Zn, O and Al can be obtained, as listed in Table 1. It was found that the as-grown AZO film is nearly stoichiometric for Zn/(O+Al). The Zn, O, and A1 amounts in the film were ~50 at.%, ~47 at.%, and ~3 at.%, respectively. Different atom percent variation behaviors were observed for the AZO films with increasing annealing temperature in different atmosphere conditions. For annealing in N_2, Zn amount in the AZO film increased, O amount decreased and Al remained unchanged with increasing annealing temperature till 600 °C. For annealing in N_2+H_2, Zn amount decreased, O increased with increasing annealing temperature till 400 °C, and

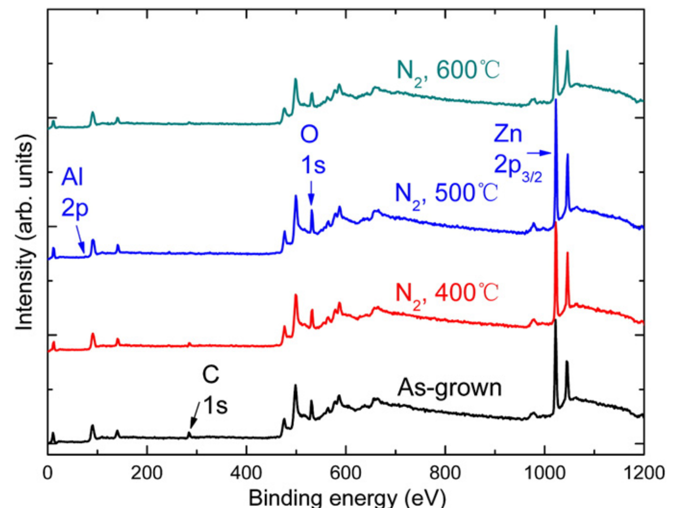

Fig. 3. XPS wide scans for the AZO films on quartz of as-grown, annealed at 400, 500 and 600 °C in N_2, respectively.

Table 2
The electrical and optical properties for the AZO films as-deposited and annealed in different atmospheres.

Sample	Resistivity (Ω cm)	Carrier concentration (cm^{-3})	Mobility (cm^2/V s)	E_g (eV)	Average transmittance (%)
As-deposited	4.60×10^{-4}	8.68×10^{20}	15.6	3.80	92.3
N_2, 400 °C	4.66×10^{-3}	2.77×10^{20}	4.44	3.59	89.2
N_2+H_2, 400 °C	5.12×10^{-4}	8.56×10^{20}	14.2	3.77	91.0
N_2, 600 °C	6.99×10^{-2}	3.22×10^{19}	2.78	3.39	84.5
N_2+H_2, 600 °C	2.69×10^{-3}	2.95×10^{20}	7.86	3.43	92.0

reversely when further increasing annealing temperature to 600 °C, i.e. Zn amount increased, O amount decreased and Al remained almost unchanged.

3.3. Electrical properties

Hall measurements were performed for the AZO films and values of electrical resistivity (ρ), carrier concentration (n), and mobility (μ) were obtained and listed in Table 2. Their dependences on annealing temperature in N_2 and $N_2+4\%$ H_2 are shown in Fig. 4. The results showed that all the films are degenerate n-type doped semiconductors. The plot in Fig. 4a) indicates the carrier concentration and mobility of AZO films decreased, while resistivity increased, with the annealing temperature increased from 300 °C to 600 °C. For annealing in N_2+H_2, the AZO films show a slight decrease of the carrier concentration and mobility and a slight increase of the resistivity with the annealing temperature from 300 °C to 500 °C, but more rapid decrease or increase from 500 °C to 600 °C. This is different from previous other reports [16–19] that the resistivity inclines to decrease after annealing. We give a detailed interpretation about the mechanism of this phenomenon later.

As can be seen in Fig. 4a) and Table 2, a resistivity value of 4.60×10^{-4} Ω cm was obtained on the as-grown AZO films, and the resistivity of the AZO films continuously increased with increasing annealing temperature in N_2, while slightly changed with annealing in N_2+H_2. The carrier concentration and the mobility of the two types of AZO films decreased with increasing annealing temperature, but the value for the AZO thin film annealed in N_2 was much smaller than for that annealed in N_2+H_2. The samples produced carrier mobility of 4.44 cm^2/V s and carrier concentrations of 2.77×10^{20} cm^{-3},

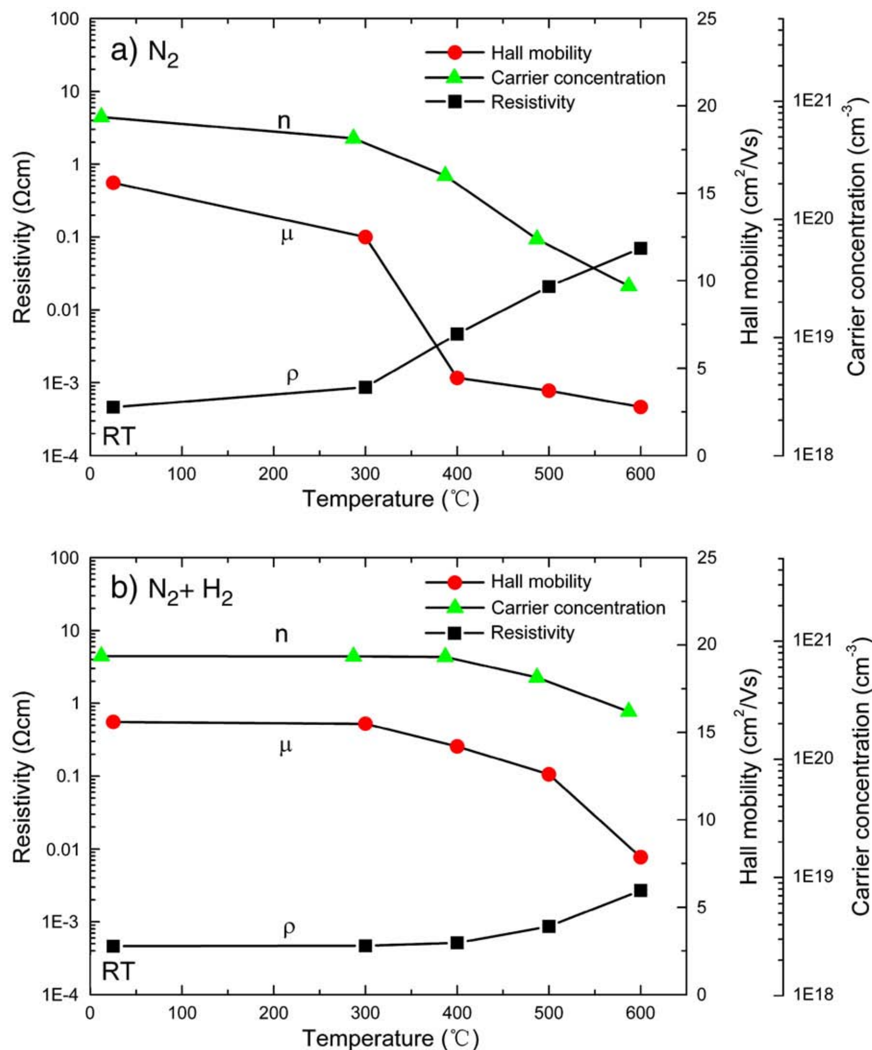

Fig. 4. Electrical properties of the AZO films as a function of the annealing temperature (resistivity = ρ, mobility = μ, and carrier concentration = n) in (a) N_2, and (b) $N_2+4\%$ H_2.

when annealed at 400 °C in N_2. However, the carrier mobility and concentration of the samples were slightly changed to 14.2 cm^2/V s and 8.56×10^{20} cm^{-3} when the samples were annealed at 400 °C in N_2+H_2.

The n-type conductivity in intrinsic ZnO is well known to originate from zinc interstitials and oxygen vacancies. When a small amount of Al was distributed into the ZnO film, the Al was ionized into Al^{3+} and substituted for Zn^{2+}. Thus, one free electron was generated from one zinc atom replacement by an aluminum atom. Thus, the electrical conductivity in AZO film in this study was primarily due to the contribution of Al ions on substitutional sites of Zn ions and Al interstitial atoms, as well as from oxygen vacancies and Zn interstitial atoms.

From comparison of these results with thermodynamic properties (Table 1), it could be speculated that the inferior electrical properties of the samples annealed in N_2 are associated with the formation of Al-oxides and reduction of carrier concentration. The decrease in the electronical properties is possibly attributed to the formation of Al–O bonds from Al ion and adsorbed oxygen at the grain boundaries. Some of Al ions will become inactive, i.e., no free electrons are released. Moreover, the Al–O bonds will impede the motion of carriers, thereby reducing their mobility.

The electrical stability of the AZO films during the hydrogen treatment is attributed to desorption of adsorbed oxygen from the grain boundaries, which will alleviate the Al ions becoming inactive. On the other hand, removal of oxygen from ZnO matrix in H_2 atmosphere will produce additional oxygen vacancies that act as donor centers in the films. However, the AZO film annealed at more than 500 °C in N_2+H_2 will be etched by H_2, it is significantly thinner than the as-grown film and the surface state density would increase greatly, as thinner films tend to have lower carrier concentration, mobility and higher resistivity values. Moreover, surface states will generate barrier and trap more electrons, the resistivity of the AZO film annealed at 600 °C in N_2+H_2 significantly increased to 2.69×10^{-3} Ω cm. Hence, the resistivities of thin films annealed in N_2+H_2 more than 500 °C may be ascribed to a combined effect of the increase of surface defects and the thinner AZO films.

3.4. Optical properties

Fig. 5 shows the optical transmittance (OT) in the wavelength range of 200–800 nm for the as-grown and post-annealed AZO thin films. All the films exhibited an average OT of 85–95% in the visible range and a sharp fundamental absorption edge. It seems that the transmittance was slightly decreased by annealing but regardless of the annealing atmosphere. The OT of a film is known to strongly depend on its surface morphology and density. This change in transmittance by annealing may be mainly attributed to more density or compact with increase of annealing temperature. Moreover, judging by the number of interference fringes in Fig. 5b), the films annealed at 600 °C in N_2+H_2 show apparently thinner than the others. This phenomenon could be explained from the AZO films in high temperature H_2 atmosphere have been etched significantly and became thinner, especially at 600 °C temperature. As we mentioned above, the surface state density would greatly increase by H_2 etching. Since surface state is related to deep level defects, which are most probably due to oxygen vacancies or zinc interstitials. The surface state level will absorb visible photons and hence reduce the OT. This can explain the phenomenon that the transmission is lower after 600 °C annealing in N_2+H_2 though the coating became thinner. These results support the analysis of electrical results and what SEM describes. However, this thickness effect was not observed for the films annealed in pure N_2, as all the fringes are aligned. And even though, annealing slightly decreased the OT of the AZO films, the films annealing in N_2+H_2 still remains an average OT of >88% in the visible range, which is suitable for display devices and solar cells as transparent electrodes.

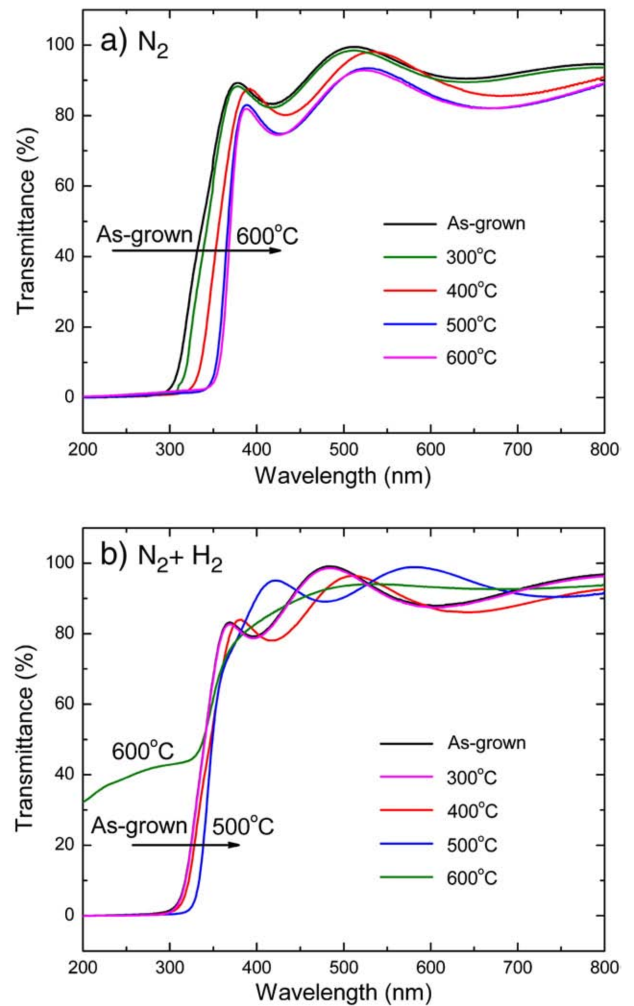

Fig. 5. Optical transmittance spectra of the AZO thin films as-grown and annealed at 300–600 °C in (a) N_2, and (b) $N_2+4\%$ H_2.

Similar to the structure of ZnO, the AZO has a direct band gap. The optical absorption edge (also named as optical energy gap), E_g, for a direct interband transition or direct band semiconductor is given by [13,20]:

$$\alpha h\nu = C(h\nu - E_g)^{1/2} \tag{2}$$

where h is the Planck constant, ν is the frequency, C is a constant and α is the optical absorption coefficient which is given from dividing absorbance by film thickness. The optical band gap (E_g) of the films can be obtained by plotting α^2 versus hν and extrapolating the linear portion of this plot to the energy axis. Fig. 6 gives examples from two pairs of AZO thin films annealed at 400 °C and 500 °C in (a) N_2, and (b) $N_2+4\%$ H_2, respectively.

The E_g of the as-grown AZO films with ~250 nm thickness is 3.80 eV, which is much larger than those reported by Kim et al. (3.46–3.54 eV) [22] and other reports from the literatures [11,14,17,20]. With increasing annealing temperature, the band gap of the AZO thin films decreased and reached 3.59 eV and 3.77 eV for annealing at 400 °C in N_2 and $N_2+4\%$ H_2 respectively. This meant the E_g of the film annealed in N_2 was greatly decreased than for that annealing in H_2. Thus, compared to the value of pure ZnO (3.30 eV), the changes of E_g implies AZO films annealing in N_2 will make partly Al^{3+} inactive and leading to lower carrier concentration, while annealing in $N_2+4\%$ H_2 makes the carrier concentration almost unchanged.

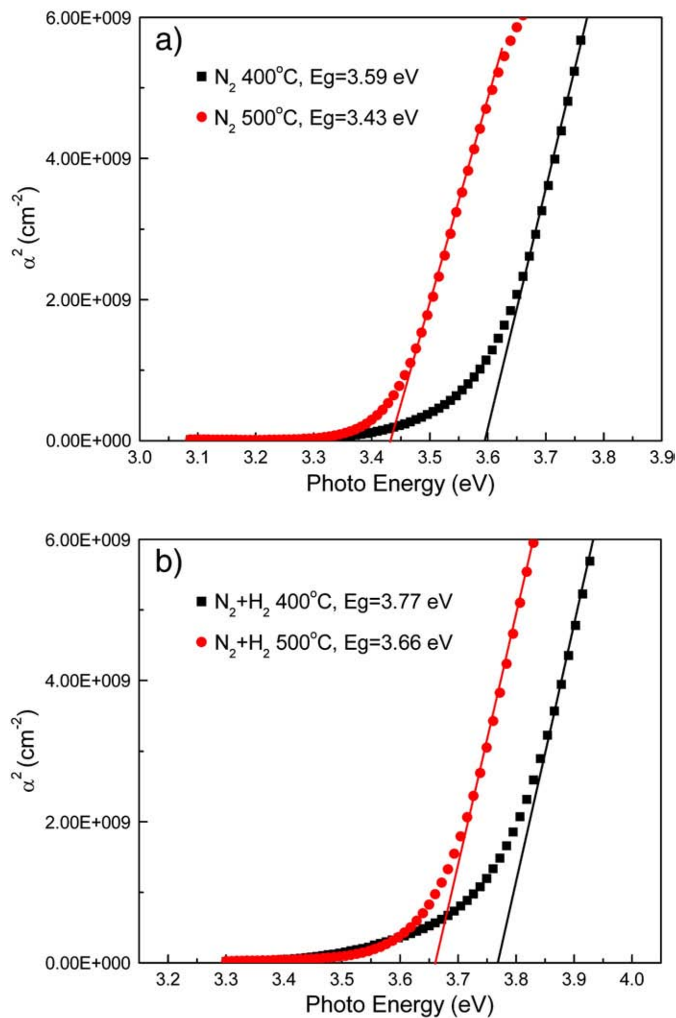

Fig. 6. Relationship of α^2 versus hν (α is the absorption coefficient and hν the photon energy) and extrapolating for optical energy gap E_g, from two pairs of AZO thin films annealed at 400 °C and 500 °C in (a) N_2, and (b) $N_2+4\%$ H_2, respectively.

As the ZnO crystal is heavily doped with Al, the optical band gap shifts to a short wavelength i.e. a high energy (blue shift), which is generally attributed to the Burstein–Moss (BM) shift [11,13,20,23]. The Fermi energy penetrates into the conduction band of the degenerate semiconductor, due to an increase in the electron concentration from Al dopants, that leads to the energy band widening [11,13]. Our experimental results from optical data in Fig. 5 predict that annealing made the optical energy gap of AZO films decrease, which is consistent with the electrical measurements in Fig. 4 and Table 2 that indicated the decrease of carrier concentration with annealing of AZO films. This means that the annealing of AZO makes the electron concentration decrease, leading to the optical gap shortening due to the BM effect [20]. Also another effect, the band gap renormalization due to many body effects may lead to a narrowing of the energy gap, which is needed to be taken into account. This band gap narrowing is competitive with the BM effects [24]. Two competing effects have made the complicated variation of the optical gap of AZO films.

4. Conclusion

In summary, high-quality transparent conducting AZO films have been grown on quartz substrates at RT by RF magnetron sputtering and the effects of thermal annealing in pure N_2 and N_2 with 4% H_2 atmosphere were studied. It was found that the crystallinity of the AZO films was improved with the annealing and that the resistivity continuously increased with increasing annealing temperature. The resistivity of the AZO thin film annealed in N_2 was higher than for that annealed in $N_2+4\%$ H_2, which implies that the low electrical resistivity of AZO thin film effectively remained by annealing in a $N_2+4\%$ H_2. This is attributed to the desorption of adsorbed oxygen from the grain boundaries and production of additional oxygen vacancies that act as donor centers by removal of oxygen from ZnO matrix. The OT of the AZO film was slightly decreased by annealing regardless of the annealing atmosphere. Annealing in $N_2+4\%$ H_2 slightly narrows the optical band gap, while annealing in an N_2 makes the band gap more narrower, which can be interpreted as a blue shift phenomenon due to the BM shift although it should also take account another competitive effect for band gap narrowing from the band gap renormalization due to many body effects. The films deposited at RT and with post-annealing in N_2+H_2 have satisfactory properties of low resistance and high transmittance for application as transparent conductive electrodes in display devices and solar cells.

References

[1] M.T. Elm, T. Henning, P.J. Klar, B. Szyszka, Appl. Phys. Lett. 93 (2008) 232101.
[2] J. Meyer, P. Görrn, S. Hamwi, H.-H. Johannes, T. Riedl, W. Kowalsky, Appl. Phys. Lett. 93 (2008) 073308.
[3] S. Cornelius, M. Vinnichenko, N. Shevchenko, A. Rogozin, A. Kolitsch, W. Möller, Appl. Phys. Lett. 94 (2009) 042103.
[4] Z.Z. Ye, L.L. Chen, B.H. Zhao, H.P. He, Appl. Phys. Lett. 92 (2008) 231913.
[5] Z. Yang, D.C. Look, J.L. Liu, Appl. Phys. Lett. 94 (2009) 072101.
[6] M.N. Jung, J.E. Koo, S.J. Oh, B.W. Lee, W.J. Lee, S.H. Ha, Y.R. Cho, J.H. Chang, Appl. Phys. Lett. 94 (2009) 041906.
[7] S.S. Lin, H.P. He, Z.Z. Ye, B.H. Zhao, J.Y. Huang, J. Appl. Phys. 104 (2008) 114307.
[8] X.H. Zhou, Q.-H. Hu, Y. Fu, J. Appl. Phys. 104 (2008) 063703.
[9] C.J. Tun, J.K. Sheu, B.J. Pong, M.L. Lee, M.Y. Lee, C.K. Hsieh, C.C. Hu, G.C. Chi, IEEE Photon. Technol. Lett. 18 (2006) 274.
[10] J. Ma, F. Ji, D.H. Zhang, H.L. Ma, S.Y. Li, Thin Solid Films 357 (1999) 98.
[11] J.P. Lin, J.M. Wu, Appl. Phys. Lett. 92 (2008) 134103.
[12] H.M. Suarez, A. Maldonado, M.D.L. Olvera, A. Reyes, R.C. Perez, G.T. Delgado, R. Asomoza, Appl. Surf. Sci. 193 (2002) 52.
[13] J. Mass, P. Bhattacharya, R.S. Katiyar, Mater. Sci. Eng. B 103 (2003) 9.
[14] S.H. Jeong, J.W. Lee, S.B. Lee, J.H. Boo, Thin Solid Films 435 (2003) 78.
[15] T. Minami, Y. Ohtani, T. Miyata, T. Kuboi, J. Vac. Sci. Technol. A 25 (2007) 1172.
[16] C.J. Tun, J.K. Sheu, M.L. Lee, C.C. Hu, C.K. Hsieh, G.C. Chi, J. Electrochem. Soc. 153 (2006) G296.
[17] J.H. Lee, B.O. Park, Mater. Sci. Eng. B 106 (2004) 242.
[18] K.K. Kim, H. Tampo, J.O. Song, T.Y. Seong, S.J. Park, J.M. Lee, S.W. Kim, S. Fujita, S. Niki, Jpn. J. Appl. Phys. 44 (2005) 4776.
[19] K.K. Kim, S. Niki, J.Y. Oh, J.O. Song, T.Y. Seong, S.J. Park, S. Fujita, S.W. Kim, J. Appl. Phys. 97 (2005) 066103.
[20] S.S. Lin, J.L. Huang, P. Šajgalik, Surf. Coat. Technol. 185 (2004) 254.
[21] W.F. Yang, Z.G. Liu, D.L. Peng, F. Zhang, H.L. Huang, Y.N. Xie, Z.Y. Wu, Appl. Surf. Sci. 255 (2009) 5669.
[22] K.H. Kim, K.C. Park, D.Y. Ma, J. Appl. Phys. 81 (1997) 7764.
[23] E. Burstein, Phys. Rev. 93 (1954) 632.
[24] J.G. Lu, S. Fujita, T. Kawaharamura, H. Nishinaka, Y. Kamada, T. Ohshima, Z.Z. Ye, Y.J. Zeng, Y.Z. Zhang, L.P. Zhu, H.P. He, B.H. Zhao, J. Appl. Phys. 101 (2007) 083705.